Astronomy & Astrophysics

Special issue

The first gradual solar energetic particle event with an enhanced 3He abundance on Solar Orbiter

R. Bučík[1], G. M. Mason[2], R. Gómez-Herrero[3], V. Krupar[4,5], D. Lario[4], M. J. Starkey[1], G. C. Ho[2], J. Rodríguez-Pacheco[3], R. F. Wimmer-Schweingruber[6], F. Espinosa Lara[3], T. Tadesse[7], L. Balmaceda[4,8], C. M. S. Cohen[9], M. A. Dayeh[1], M. I. Desai[1], P. Kühl[6], N. V. Nitta[10], M. E. Wiedenbeck[11], and Z. G. Xu[6]

[1] Southwest Research Institute, San Antonio, TX 78238, USA
  e-mail: radoslav.bucik@swri.org
[2] Applied Physics Laboratory, Johns Hopkins University, Laurel, MD 20723, USA
[3] Universidad de Alcalá, Space Research Group, 28805 Alcalá de Henares, Spain
[4] Heliophysics Science Division, NASA Goddard Space Flight Center, Greenbelt, MD 20771, USA
[5] Goddard Planetary Heliophysics Institute, University of Maryland, Baltimore, MD 21250, USA
[6] Institut für Experimentelle und Angewandte Physik, Christian-Albrechts-Universität zu Kiel, Kiel, Germany
[7] NASA Johnson Space Center, Houston, TX 77058, USA
[8] George Mason University, Fairfax, VA 22030, USA
[9] California Institute of Technology, Pasadena, CA 91125, USA
[10] Lockheed Martin Advanced Technology Center, Palo Alto, CA 94304, USA
[11] Jet Propulsion Laboratory, California Institute of Technology, Pasadena, CA 91109, USA

ABSTRACT

The origin of ^{3}He abundance enhancements in gradual solar energetic particle (SEP) events remains largely unexplained. Two mechanisms have been suggested: the reacceleration of remnant flare material by coronal mass ejection (CME)-driven shocks in interplanetary space, and concomitant activity in the corona. We explore the first gradual SEP event with enhanced ^{3}He abundance that was observed by Solar Orbiter. The event started on 2020 November 24 and was associated with a relatively fast halo CME. During the event, the spacecraft was at 0.9 au from the Sun. The event-averaged ^{3}He/^{4}He abundance ratio is 24 times higher than the coronal or solar wind value, and the timing of the ^{3}He intensity was similar to that of other species. We inspected available imaging, radio observations, and the spacecraft magnetic connection to the CME source. The most probable cause of the enhanced ^{3}He abundance apparently are residual ^{3}He ions remaining from a preceding long period of ^{3}He-rich SEPs on 2020 November 17–23.

Key words. Sun: particle emission – Sun: abundances – Sun: flares – Sun: coronal mass ejections (CMEs) – acceleration of particles

1. Introduction

Solar energetic particles (SEPs) are produced by mechanisms related to magnetic reconnection in flares or jets in impulsive SEP (ISEP) events and by coronal mass ejection (CME)-driven shocks traveling through the corona and interplanetary space in gradual SEP (GSEP) events (e.g., Reames 2021b). One of the most strikingly distinct characteristics of these groups is their different elemental composition (e.g., Reames 2021a). ISEP (or ^{3}He-rich) events have higher ^{3}He and heavy-ion abundances than are found in the corona or in the solar wind (e.g., Mason 2007), while the abundances of GSEP events are similar to coronal values (e.g., Desai & Giacalone 2016). High-resolution mass spectrometers on board the Advanced Composition Explorer (ACE) have often revealed small enhancements of ^{3}He and Fe abundances in GSEP events (e.g., Mason et al. 1999a,b; Cohen et al. 1999; Wiedenbeck et al. 2000; Desai et al. 2016), thus blurring the distinction between jet- and CME-related SEPs. While the Fe/O enhancement in GSEP events can result from magnetic rigidity-dependent transport effects due to the lower charge-to-mass ratio of Fe compared to O, this effect is not expected for ^{3}He/^{4}He enhancement (e.g., Mason et al. 1999b). Thus, a ^{3}He enhancement unambiguously

indicates the presence of flare material in GSEP events (e.g., Desai et al. 2016).

Mason et al. (1999a) reported two GSEP events on 1997 November 4 and November 6 with a 0.5–2.0 MeV nucleon^{-1} ^{3}He/^{4}He ratio that was higher by a factor of 4 than the average solar wind value of $(4.8\pm0.5)\times10^{-4}$ (Ogilvie et al. 1980). Mason et al. (1999b) examined 12 GSEP events and found a finite 0.5–2.0 MeV nucleon^{-1} ^{3}He peak in 8 events with a ^{3}He/^{4}He ratio that was from 4.7 to 135 times the average slow solar wind ^{3}He/^{4}He of $(4.08\pm0.25)\times10^{-4}$ (Gloeckler & Geiss 1998). The 0.4–0.6 MeV nucleon^{-1} Fe/O ∼ 0.79 was also enhanced compared to the average GSEP value. The 5 events in Mason et al. (1999b) showed similar ^{3}He and ^{4}He time-intensity profiles, indicating a common acceleration and transport origin. These authors suggested that residual ^{3}He ions from ISEP events, which were found to be commonly present in the interplanetary medium at 1 au, form a source material for the ^{3}He that is observed in GSEP events. Similarly, Tylka et al. (2005) proposed that enhanced Fe/O in GSEP events may be produced by the acceleration of a remnant suprathermal Fe-rich ion population from previous small flare events. Desai et al. (2016) identified 27 out of 46 GSEP events with a finite ^{3}He mass peak and a 0.5–2.0 MeV nucleon^{-1} ^{3}He/^{4}He ratio between ∼1.5 and ∼194

times the average slow solar wind value (Gloeckler & Geiss 1998). A flare component that is simultaneously produced in the parent active regions (ARs; Von Rosenvinge et al. 2000; Cane et al. 2003, 2006; Ko et al. 2013) or in other sites in the corona (Ko et al. 2013) has been proposed as cause of the Fe/O and ^{3}He/^{4}He enhancement in GSEP events. The longitude of the observer relative to the source AR (Cane et al. 2003) and the nature of the photospheric field to which the observer is magnetically connected (Ko et al. 2013) have also been suggested to affect the Fe/O ratio.

The unresolved question of whether residual flare material in interplanetary space or concomitant coronal activity dominates ^{3}He abundance enhancements in GSEP events can be thoroughly explored with new high-resolution in situ and remote measurements from Solar Orbiter (Müller 2020) at close distances from the Sun. In this study, we investigate the first GSEP event with enhanced ^{3}He abundance measured by Solar Orbiter and analyze the origin of the observed ^{3}He enhancement. The event started on 2020 November 24. It is also the first significant SEP event observed by this mission that has high proton intensities. At suprathermal energies (<1 MeV nucleon^{-1}), this event shows higher proton intensities than the following SEP event on 2020 November 29 (Kollhoff et al. 2021), which was observed at widely (~230°) separated spacecraft and is associated with the same AR as the 2020 November 24 event.

2. Instrumentation

The 2020 November 24 event abundance measurements were obtained by the Suprathermal Ion Spectrograph (SIS) of the Energetic Particle Detector (EPD) suite (Rodríguez-Pacheco et al. 2020) on board Solar Orbiter. SIS is a time-of-flight mass spectrometer that measures elemental composition from H through ultra-heavy nuclei in the kinetic energy range of ~0.1–10 MeV nucleon^{-1}. SIS has two telescopes, one (SIS-A) pointing at 30° (sunward) and the other (SIS-B) at 160° (anti-sunward) to the west of the spacecraft-Sun line. The energetic proton measurements were obtained from the High-Energy Telescope (HET) of the EPD suite. HET has four viewing directions, with one unit pointing sun- and anti-sunward along the average Parker spiral, and the other unit pointing out of the ecliptic. We also used electron measurements from EPD made by the SupraThermal Electron Proton (STEP), Electron Proton Telescope (EPT), and HET instruments. To determine the interplanetary magnetic field (IMF) polarity, we used magnetic field data from the magnetometer (MAG) on board Solar Orbiter (Horbury et al. 2020).

The coronal activity associated with the event was examined using extreme-UV (EUV) and white-light images from the EUV imager (EUVI) and COR2 coronagraph on Solar Terrestrial Relations Observatory A (STEREO-A; Howard et al. 2008). Solar Orbiter EUV imaging observations from the Extreme Ultraviolet Imager (EUI; Rochus et al. 2020) were not available for the 2020 November 24 event. Furthermore, we inspected radio data from the STEREO-A/WAVES (Bougeret et al. 2008) and the Solar Orbiter Radio and Plasma Waves (RPW; Maksimovic et al. 2020) instruments.

3. Observations

The selection of the examined event as a GSEP event is primarily based on abundance ratios that are comparable with the reference population. Furthermore, the event is associated with a large and fast CME, which is typically observed in GSEP events. Figure 1
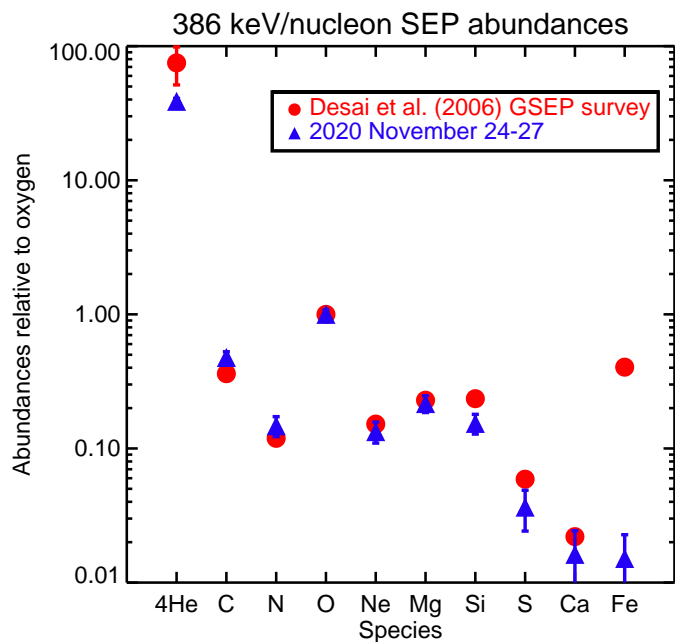

Fig. 1. Abundances relative to O for the 2020 November 24 event (blue triangles). Reference ion abundances (red circles) are from the GSEP event survey by Desai et al. (2006).

displays an abundance plot for the event and reference population obtained in the GSEP survey by Desai et al. (2006).

3.1. Solar energetic ions

Figure 2 (left) shows the locations of selected spacecraft in the plane of the ecliptic as seen from the north on 2020 November 24 at 12:30 UT in heliocentric Earth ecliptic (HEE) coordinates. The dashed Parker spiral connects to the CME source longitude (E105 with respect to STEREO-A) as inferred from EUV STEREO-A observations (see Sect. 3.2 below). Solar Orbiter is well connected to the CME source site along a nominal Parker spiral IMF line. The angular separation between the Solar Orbiter magnetic footpoint longitude on the Sun and the longitude of the CME source is ~15° for a nominal Parker spiral for a 350 km s^{-1} solar wind speed. We note that the solar wind measurements from the Solar Orbiter Solar Wind Analyser (SWA; Owen et al. 2020) are not available for the period of interest. The event was also observed by Parker Solar Probe (PSP), but neither by STEREO-A nor by spacecraft located near Earth (e.g., ACE). The longitudinal separation between Solar Orbiter and PSP of 144° suggests widespread SEPs in the event. Solar Orbiter was at 0.9 au and PSP at 0.8 au from the Sun. The EPD/HET Solar Orbiter 1 hr omnidirectional proton intensities at 10 and 50 MeV for the examined event are displayed in Fig. 2 (right). There is no measured intensity enhancement at 50 MeV. The rapid onset of the event, seen just after the vertical dashed line marking the first appearance of the CME in the coronagraph, is preceded by a small proton enhancement at ~07 UT. There have been reports of EPD electron enhancements with onset at 06:51 UT at 53–85 keV (Wimmer-Schweingruber et al. 2021), which is likely related to this small proton event.

Figure 3 shows Solar Orbiter SIS measurements of the event on 2020 November 24–27. Figure 3a displays 1 h H, ^{3}He, ^{4}He, O, and Fe intensity at 0.23–0.32 MeV nucleon^{-1}. The 1 hr ^{3}He intensity is plotted only if the 0.23–0.32 MeV nucleon^{-1}
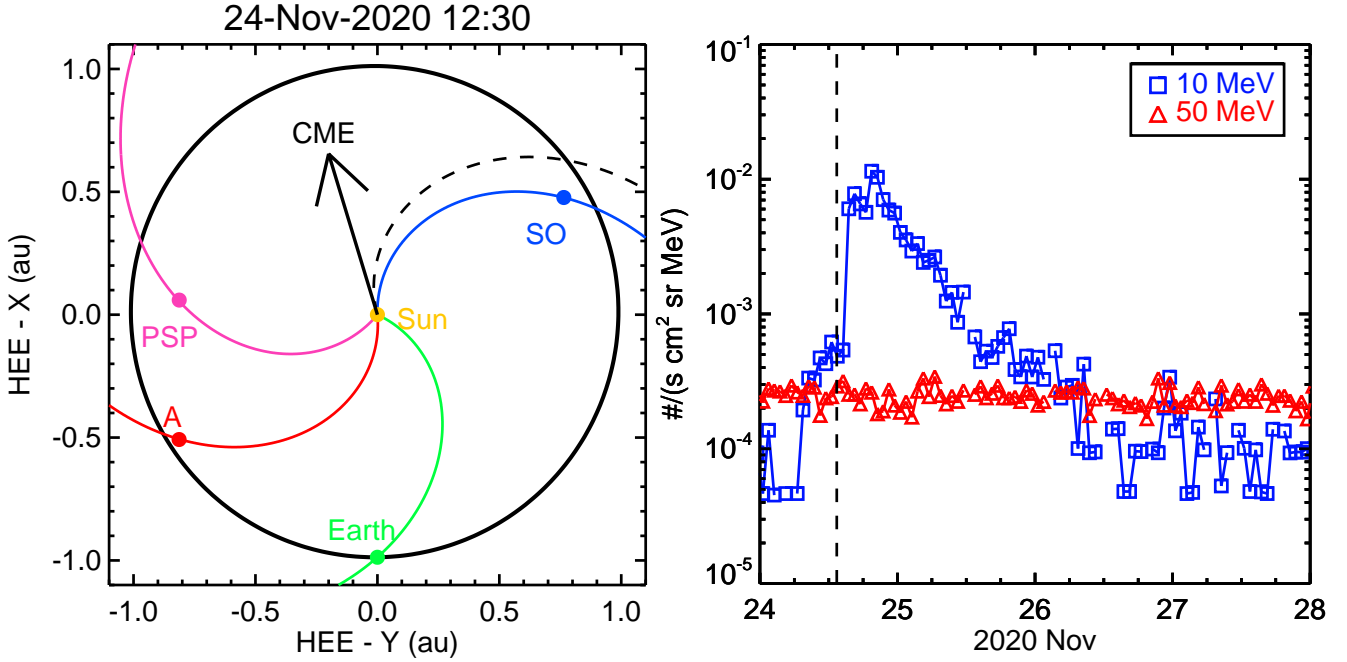
Fig. 2. Constellation of selected spacecraft and high-energy proton observation of the GSEP event. Left: blue, pink, red, and green circles mark the heliocentric Earth ecliptic (HEE) location of Solar Orbiter (SO), Parker Solar Probe (PSP), STEREO-A (A), and Earth, respectively, on 2020 November 24 at 12:30 UT. The arrow indicates the estimated longitude of the CME source. Nominal Parker spiral IMF lines assuming a 350 km s^{-1} solar wind speed are shown. Right: Solar Orbiter EPD/HET 1 h omnidirectional proton intensity, obtained by averaging the intensities of the four telescopes. The curve with blue squares, marked 10 MeV, is a combination of 11 energy bins between 7.0 and 11.3 MeV, and the curve with red triangles, marked 50 MeV, is a combination of 13 energy bins between 27.2 MeV and 75.1 MeV. The vertical dashed line indicates the first appearance of the CME in the STEREO-A/COR2 coronagraph.

^{3}He/^{4}He ratio is above 5%, and there are more than eight ^{3}He counts throughout the 1 h interval. The small H intensity enhancement that precedes the main event is also seen at 0.23–0.32 MeV nucleon^{-1} around midday of November 24, which agrees with the ~10 MeV onset at ~07 UT. The intensities of the heavier ions were too low to be detected along with H. The 2020 November 24 event was only marginally (compared to Solar Orbiter) observed on PSP, with an approximate order of magnitude increase above the pre-event background. The event on PSP was clearly seen at energies below ~0.2 MeV with a velocity dispersive profile. We overplot in Fig. 3a the 1 hr H count rates summed over 14 energy bins between 0.023 MeV and 0.187 MeV from PSP Integrated Science Investigation of the Sun (IS☉IS) EPI-Lo instrument (Hill et al. 2017) with a gray line. The elements with $Z > 2$ were not measured on PSP in this event. The Solar Orbiter SIS ^{4}He/H and Fe/O ratios at 0.23–0.32 MeV nucleon^{-1} shown in Fig. 3b are close to GSEP event values. The ^{4}He/H and Fe/O in ISEP events are about ten times higher (e.g., Reames 1995). The Solar Orbiter SIS mass spectrogram (Fig. 3c) shows a clear ^{3}He presence and an almost complete lack of Fe during the event at energy 0.4–10 MeV nucleon^{-1}. A few ^{3}He ions detected on November 24, just before the event, may be remnants from a long period of ^{3}He-rich SEPs measured with SIS on board Solar Orbiter on November 17–23 (see the left panel of Fig. 4 and also Bučík et al. 2021). The 1/ion-speed vs. time plot (Fig. 3d) shows a dispersive triangular pattern in which a rough extrapolation to zero of the inverted speed suggests an ion solar release time around 13:00 UT. Previous studies reported an uncertainty of ±45 min in estimates of release times from low-energy <1 MeV nucleon^{-1} measurements (e.g., Mason et al. 2000). The horizontal color bar at the top of Fig. 3 shows the IMF polarity

determined from 10-min Solar Orbiter MAG data. Red denotes IMF azimuthal angles 90°–180°, which typically correspond to toward or negative polarity. Green denotes angles 270°–360° (away or positive polarity). Yellow marks the remaining angles, which have an ambiguous polarity.

Figure 4 (left) displays the He mass spectrogram for the period 2020 November 17–23 (Bučík et al. 2021). Figure 4 (right) shows the event-integrated ^{4}He/H (blue) and Fe/O (orange) as a function of energy. The Fe/O spectrum only extends to ~0.3 MeV nucleon^{-1} due to the lack of Fe counts above 0.4 MeV nucleon^{-1} (Fig. 3b). The ^{4}He/H is close to or lower than the GSEP value of ~0.01 (e.g., Reames 1995; Kahler & Brown 2021). The Fe/O is close to or higher than the GSEP value of ~0.1, but does not reach the ISEP value of ~1 (e.g., Reames 1995). A decrease of ^{4}He/H and Fe/O with increasing kinetic energy has previously been reported in GSEP events (e.g., Desai & Giacalone 2016).

The He mass histogram in Fig. 5 (left) shows a clear ^{3}He peak that is well separated from the ^{4}He peak. The event-integrated 0.5–2.0 MeV nucleon^{-1} ^{3}He/^{4}He ratio of 0.0094±0.0014 is ~23.5 times higher than the average ^{3}He/^{4}He of (4.08±0.25)×10^{-4} in the slow solar wind (Gloeckler & Geiss 1998). Figure 5 (right) shows time profiles of 0.4–10 MeV nucleon^{-1} 1 h ^{4}He and 6 h ^{3}He count rates. We used 2.8–3.2 AMU and 3.3–6 AMU mass ranges for ^{3}He and ^{4}He count rates, respectively. ^{4}He data points with one count are not plotted. ^{3}He data points with one count are shown, and their error bars are marked by an arrow. The time profile of the ^{3}He count rate is similar to the ^{4}He time profile, except for a few ^{3}He points with large errors near the end of the event. It has been argued that this similarity suggests the same acceleration and propagation histories (e.g., Mason et al. 1999b; Wiedenbeck et al. 2000).
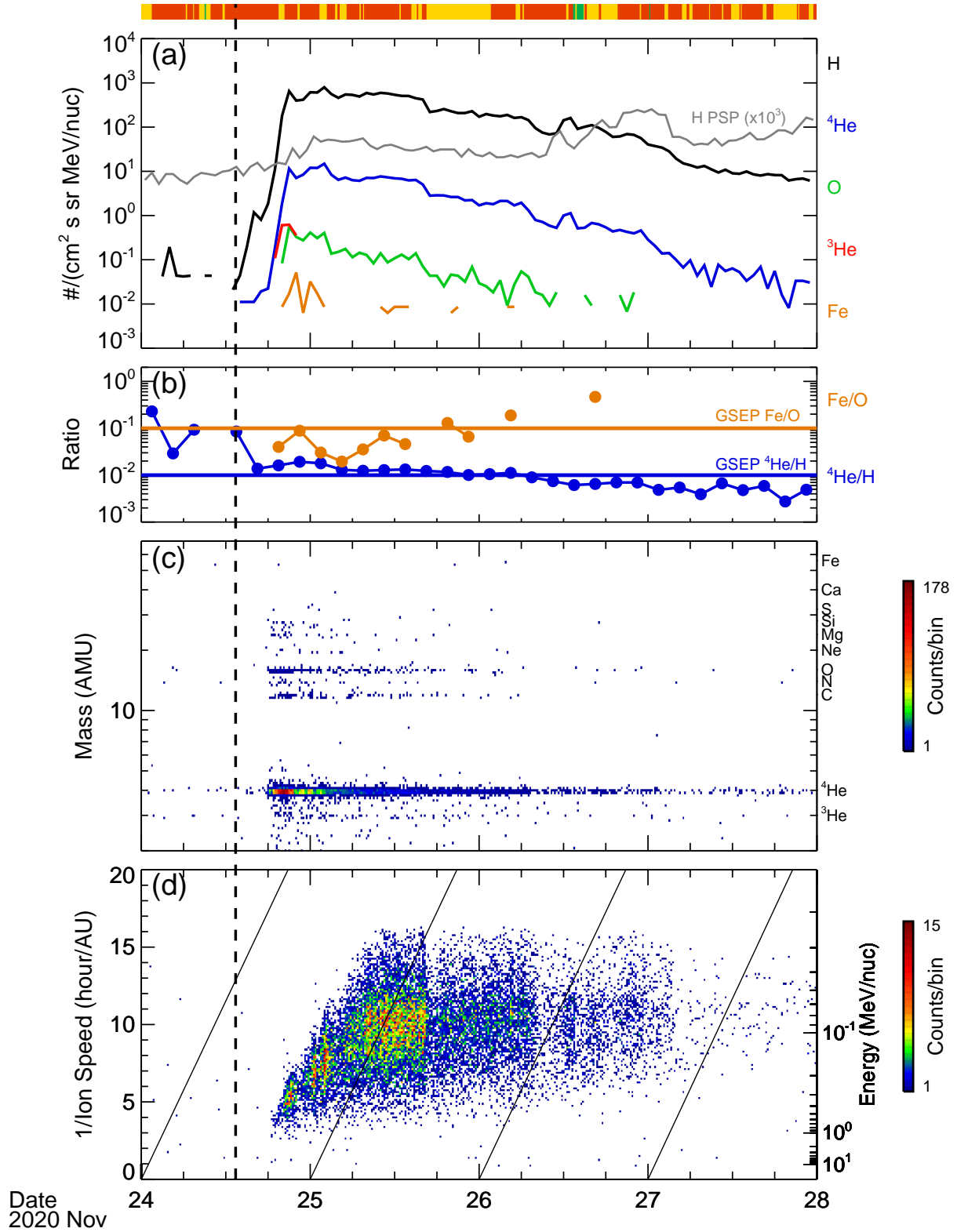
Fig. 3. GSEP event with time profiles of various physical quantities. (*a*) Solar Orbiter SIS 1 hr H, ^{3}He, ^{4}He, O, and Fe intensity at 0.23–0.32 MeV nucleon^{-1}. The H PSP curve is a combination of 1 hr H count rates (s^{-1}) from 14 energy bins between 0.023 MeV and 0.187 MeV from PSP IS☉IS EPI-Lo. (*b*) Solar Orbiter SIS 3 h ^{4}He/H and Fe/O ratios at 0.23–0.32 MeV nucleon^{-1}. The horizontal lines mark ^{4}He/H and Fe/O in GSEP events (Reames 1995). (*c*) Solar Orbiter SIS mass vs. time at 0.4–10 MeV nucleon^{-1}. (*d*) Solar Orbiter SIS 1/(ion speed) vs. arrival times of 10–70 AMU ions. The measurements are from both SIS telescopes and averaged together. The vertical dashed line indicates the first appearance of the CME in the STEREO-A/COR2 coronagraph. Sloped lines mark arrival times for particles traveling along the nominal Parker field line without scattering. The horizontal color bar on the *top* shows IMF polarity at Solar Orbiter. Red is negative, green is positive, and yellow is an ambiguous polarity.
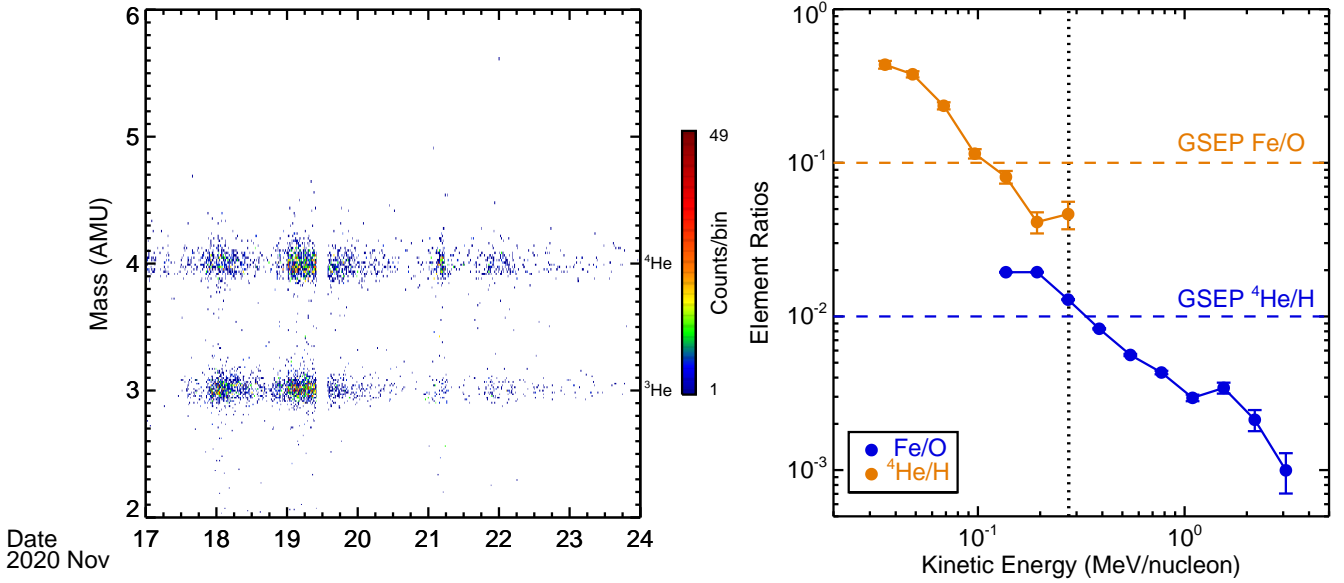
Fig. 4. Long period of ^{3}He-rich SEPs and energy dependence of selected abundance ratios. Left: Solar Orbiter SIS He mass vs. time at 0.4–10 MeV nucleon^{-1}. The sharp cutoff of particles around midday on November 19 was due to instrument maintenance. Right: event-integrated element ratios Fe/O and ^{4}He/H over the period of 2020 November 24 12:00 UT–2020 November 27 00:00 UT vs. energy. The vertical dotted line marks the energy corresponding to the ratios in Fig. 3b. The measurements are from both SIS telescopes averaged together.
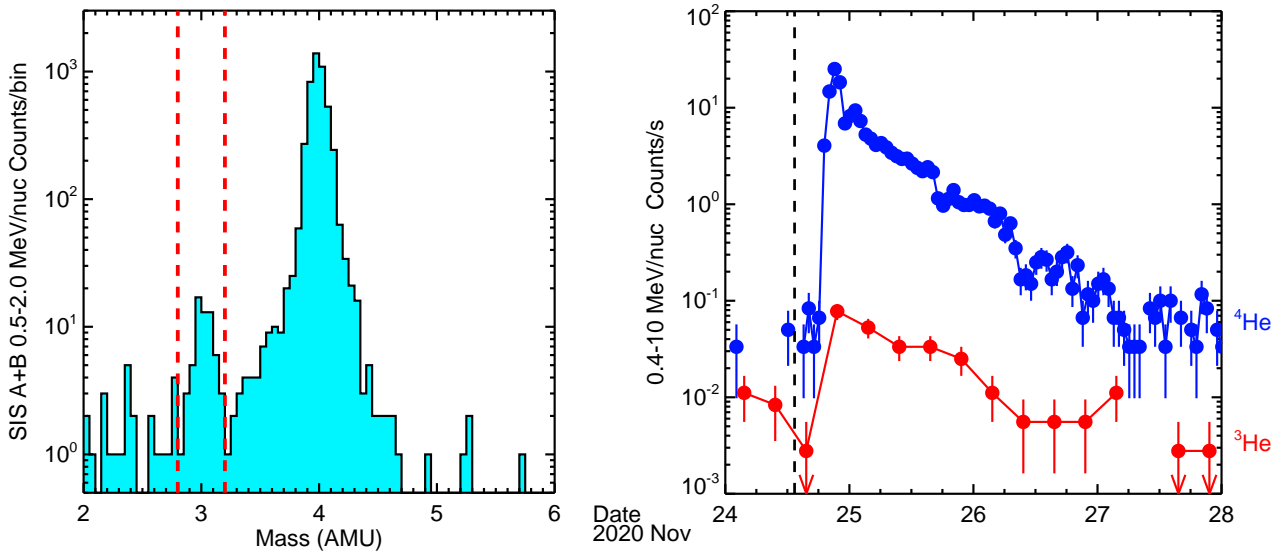

Fig. 5. ^{3}He mass peak and comparison of ^{3}He and ^{4}He counts s^{-1} time profiles. *Left*: He mass histogram from the two SIS telescopes A and B for 2020 November 24 12:00 UT–2020 November 27 00:00 UT and energy range of 0.5–2.0 MeV nucleon^{-1}. The vertical dashed red lines mark the mass range for ^{3}He count rates shown in the *right panel*. *Right*: SIS 1 h ^{4}He and 6 h ^{3}He count rates at 0.4–10 MeV nucleon^{-1}. The vertical dashed black line indicates the first appearance of the CME in the coronagraph.

Figure 5 (right) also shows that the ^{3}He count rates increase significantly compared to the pre-event ^{3}He background.

3.2. Solar source

The examined SEP event is related to the partial halo CME with a reported speed of 892 km s^{-1} and width of 106° that appeared in the COR2 coronagraph on board STEREO-A on 2020 November 24 at 13:24 UT, consistent with the estimated ion injection time at ~13 UT. These values are from the automatically generated list of CMEs[1] of STEREO-A

(Robbrecht et al. 2009), which uses images from the COR2 coronagraph (field of view of 2.5–15 $R_\odot$). The Solar and Heliospheric Observatory (SOHO) Large Angle and Spectrometric Coronagraph Experiment (LASCO) manually identified CME catalog[2] (Yashiro et al. 2004) reports a halo CME with a speed of 668 km s^{-1} that appeared in the C2 coronagraph (1.5–6 $R_\odot$) on 2020 November 24 at 13:25 UT. Figure 6 (top row) shows the CME expulsion between 12:20 and 12:35 UT on November 24 in STEREO-A EUV images from EUVI, whose field of view extends to 1.7 $R_\odot$. The CME eruption started around 12:25 UT from the area near ~S20 at the east limb as viewed from

---

[1] https://secchi.nrl.navy.mil/cactus/

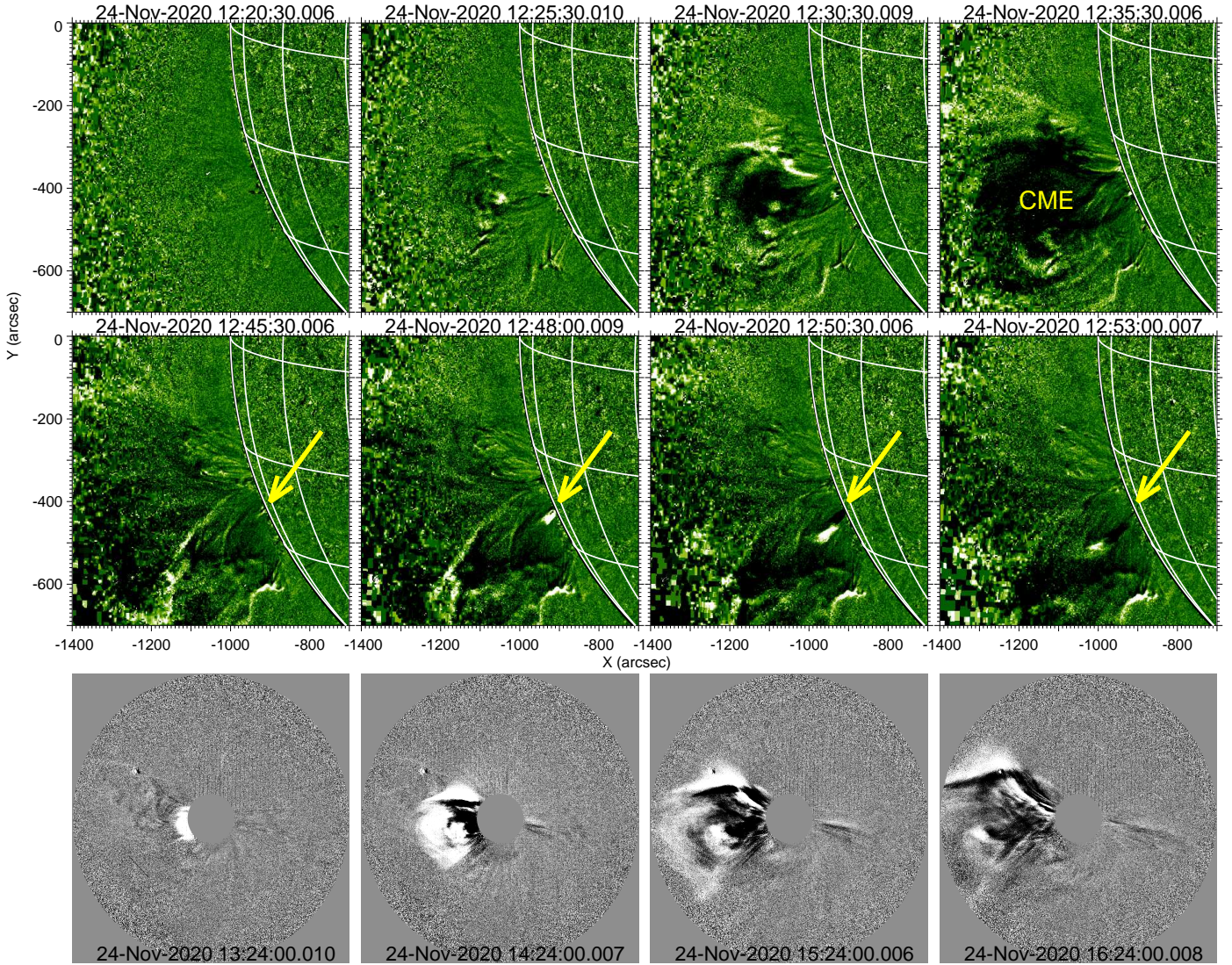[2] https://cdaw.gsfc.nasa.gov/CME_list/

Fig. 6. CME and jet expansion. *Top and middle panel*: STEREO-A EUVI 2.5-min running-difference EUV 195 Å images. The arrows mark the post-CME jet-like ejection. The heliographic longitude-latitude grid has a spacing of 15°. *Bottom*: STEREO-A COR2 30-minute running-difference white-light images.

STEREO-A. In the same area, STEREO-A EUVI began to observe a small CME post-eruptive arcade (not shown) at ~14:00 UT on November 24, indicating that the CME source was close to the east limb. On November 26, STEREO-A spotted the AR (number 12790) in which the CME originated. An estimated location of the AR was S25E105 (from the point of view of STEREO-A) at the time of the CME eruption. A jet-like eruption occurred ~20 min after CME, apparently from the same area and in the same projected direction as the CME (Fig. 6, middle row arrow). Figure 6 (bottom row) shows the progression of the CME in the COR2 coronagraph.

Figure 7 shows full-disk STEREO-A EUV daily images between 2020 November 24 and November 27. The above-mentioned jet is marked in the leftmost panel. The large bright area that passed through the central meridian represents ARs 12786 and 12785, the sources of a long period of ^{3}He-rich SEPs (Bučík et al. 2021). AR 12790, in which the CME (and probably the jet) originated, is marked in the two rightmost panels.

Figure 8 displays a photospheric magnetic field map with a potential field source surface (PFSS; Schatten et al. 1969) model

coronal field around the onset of the CME. The PFSS model presents a simple approximation to the real global coronal field that neglects the effects of the forces and electric currents. The PFSS model was computed using the SolarSoft PFSS package, which uses the Solar Dynamics Observatory Helioseismic and Magnetic Imager line-of-sight magnetograms. The magnetograms are assimilated into the flux-dispersal model to provide the magnetic field on the full solar sphere (Schrijver & De Rosa 2003). The source surface that separates open and closed fields was set to the commonly used $2.5\,R_\odot$ from the center of the Sun. Figure 8 shows that the Solar Orbiter magnetic footpoint longitude (blue triangle) for a nominal solar wind speed of $350\,\mathrm{km\,s^{-1}}$ was close to the longitude of the CME source AR 12790. Furthermore, Solar Orbiter might be connected to AR 12790 via open negative-polarity coronal field lines emanating from the AR. We note that the in situ IMF polarity on Solar Orbiter (see Fig. 3) is consistent with the model prediction. The PSP footpoint (pink square) separation of ~120° from the CME source AR might be the reason for the only small intensity increase that was observed on the spacecraft.
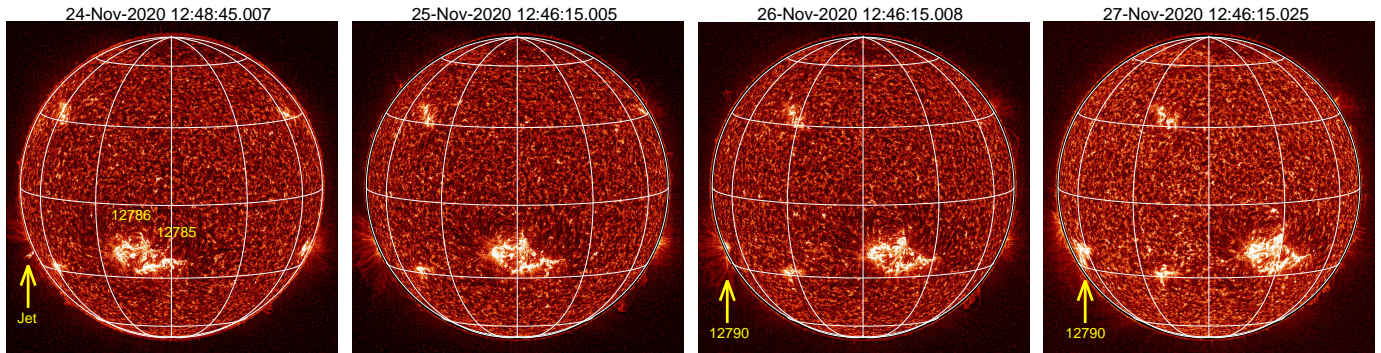
Fig. 7. CME source AR and jet in full-disk solar images. STEREO-A EUVI direct EUV 304 Å images. The heliographic longitude-latitude grid has a spacing of 30°.
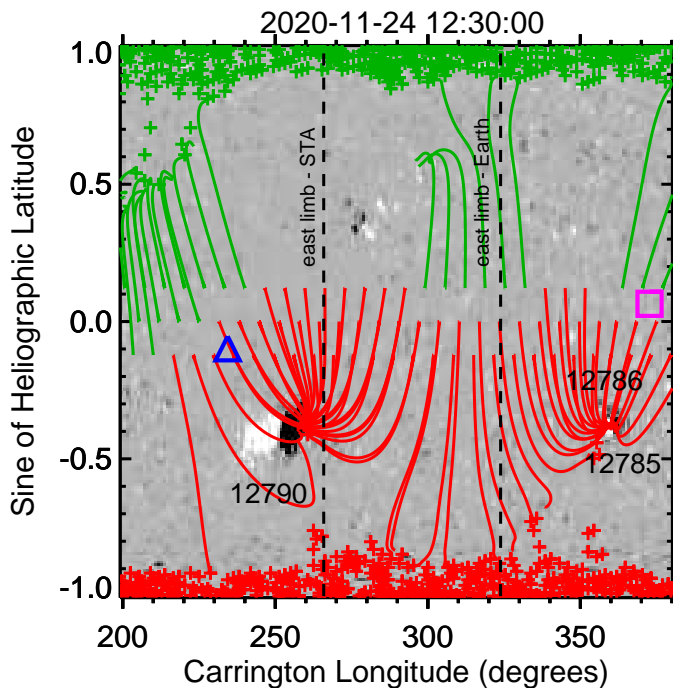

Fig. 8. Magnetic field map with a coronal field model. Photospheric magnetic field, scaled to ±30 Mx cm^{-2} (grayscale), and PFSS model coronal field (red is the negative and green is the positive polarity). We show field lines that intersect the source surface at latitudes 0°and ±7°. The blue triangle marks Solar Orbiter, and the pink square marks PSP magnetic footpoints at the source surface. The two dashed vertical lines mark the Carrington longitudes of the east solar limb as viewed from STEREO-A (STA) and the Earth.

Figure 9 (top and middle) displays STEREO-A/WAVES and Solar Orbiter/RPW radio spectrograms with times shifted to the Sun. They cover the period of the CME and the jet. The two spectrograms show a markedly different appearance. STEREO-A saw storm type III bursts at a frequency range from ~5 MHz to ~300 kHz. The jet start time, shifted to the Sun, is marked by the second vertical solid line in the top panel. There is very likely a coincidental observation of a storm type III at 12:45 UT with the jet at STEREO-A, otherwise, we would see this type III burst also on Solar Orbiter. Thus, no clear type III burst association with the solar jet can be found. In the period covered by Fig. 9, Solar Orbiter observed a single type III radio burst starting at 13:18 UT (or at 13:11 UT shifted to the Sun) and drifting from ~2 MHz (corresponding to ~6 $R_\odot$; Mann et al. 1999) to the local

plasma frequency (~30 kHz). The start time of the type III burst, marked by an arrow in the middle panel, immediately precedes the first appearance of the CME in the COR2, marked by the vertical dashed line in the top panel. Figure 9 (bottom) displays Solar Orbiter electron c/v vs. time spectrogram. This was formed using STEP, EPT, and HET data (top to bottom), which shows a dispersive energetic electron event. Although the observations are limited by the relatively low statistics, the inferred electron solar release time (SRT) at 13:09:41 UT agrees well with the type III burst onset shifted to the Sun at 13:11 UT.

Type III storms were observed by STEREO-A throughout 2020 November 23–29. They probably originated in the closely spaced ARs 12785 and 12786 (see Fig. 7), which showed a persistent brightening. As these regions rotated out of the STEREO-A view, the storm activity decreased.

4. Discussion

We examined the first intense GSEP event with an enhanced ^{3}He abundance measured on Solar Orbiter. The ^{3}He abundance is significantly (by a factor of ~24) enhanced above the coronal or solar wind abundance. The fundamental question concerning the origin of the ^{3}He in the examined event is whether this ^{3}He enhancement is due to remnant material left in the heliosphere or to simultaneous activity in the corona (e.g., a parent AR).

The timeline of the solar events is summarized in Table 1. Column 1 shows the type of activity. The instruments that observed the activity are given in parentheses. Columns 2 and 3 give the observed approximate times and the times shifted to the Sun, respectively.

A jet-like expulsion (see Fig. 6) was observed to closely follow (after ~20 min) the CME liftoff. If ^{3}He-rich SEPs were produced in association with this jet, ions with kinetic energy, for instance, 0.23–0.32 MeV nucleon^{-1}, would arrive at Solar Orbiter at ~19–20 UT (assuming a nominal Parker spiral), which is consistent with the timing of the measurements of ^{3}He in the event. However, no type III radio bursts (Fig. 9, middle), a signature of energetic electron production and escape, or energetic electrons (see Fig. 9, bottom) were observed in association with the jet. We recall that the type III radio burst and the electron event observed by Solar Orbiter are significantly later than the start of the jet. It is known that ^{3}He-rich SEP events show a strong (~99%) association with type III radio bursts (e.g., Nitta et al. 2006), and only a few cases have been reported without type III bursts (Mason et al. 2009). Thus, it is unlikely that ^{3}He was produced in the jet-like eruption.
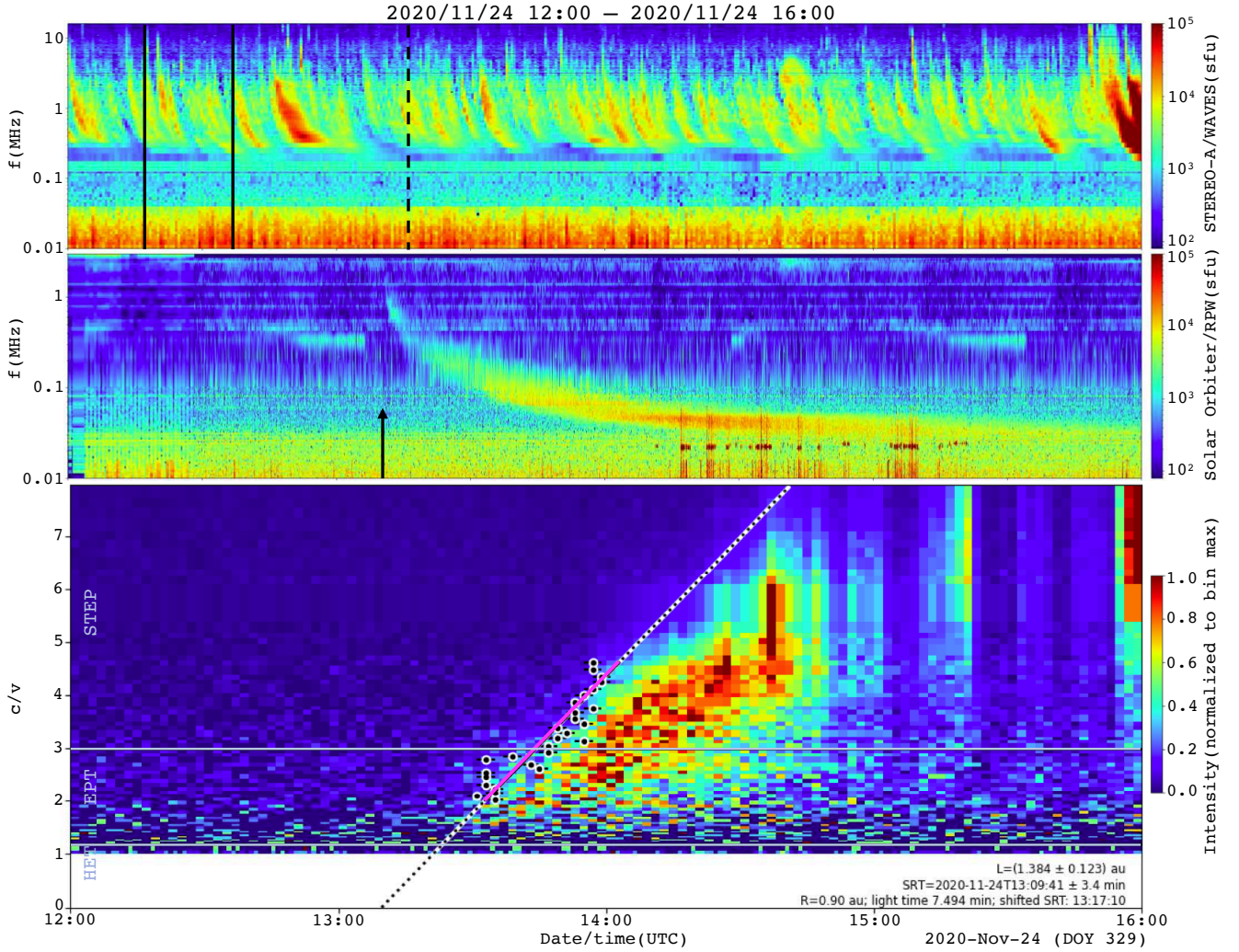
Fig. 9. Radio and electron spectrograms. *Top*: STEREO-A WAVES and (*middle*) Solar Orbiter RPW radio spectrograms with times shifted to the Sun. The two vertical solid lines mark the start of the CME and jet-like eruptions in EUVI, respectively. The vertical dashed line marks the first appearance of the CME in COR2. The arrow marks the onset of the type III radio bursts at 13:18 UT observed by Solar Orbiter. We note that all vertical lines in the *top panel* and the arrow in the *middle panel* mark times shifted to the Sun. *Bottom*: electron c/v vs. time plot, where c is the speed of light and v is the electron velocity. The slanted line is a linear fit to the electron arrival times; the solid part of the line marks the energy range used for the fit. Gray horizontal lines separate the STEP, EPT, and HET energy ranges.

Table 1. Timeline of solar events.

Activity	Observed time (UT)	Time at Sun (UT)
CME start (EUVI)	2020-Nov.-24 12:25	2020-Nov.-24 12:17
Jet start (EUVI)	2020-Nov.-24 12:45	2020-Nov.-24 12:37
Ion injection (EPD)	…	2020-Nov.-24 13:00
Electron injection (EPD)	…	2020-Nov.-24 13:09
Type III burst (RPW)	2020-Nov.-24 13:18	2020-Nov.-24 13:11
CME appearance (COR2)	2020-Nov.-24 13:24	2020-Nov.-24 13:16

On its way from the Sun, the event-associated CME shock wave can accelerate remnant ^{3}He from a heliospheric reservoir. The reservoir creation requires ^{3}He injections and preceding magnetic disturbances, such as interplanetary CMEs, that inhibit particle escape (e.g., Roelof et al. 1992; Reames 2013). The long period of energetic ^{3}He on 2020 November 17–23 (Fig. 4 left) was caused by at least five ion injections: three on November 17, one on November 18, and one on November 20 (Bučík et al. 2021). The source in question rotated from E90 to E50 (viewed from STEREO-A), thus filling a substantial volume in the heliosphere with ^{3}He. The median values of ^{3}He/^{4}He and Fe/O at 0.2–2.0 MeV nucleon^{-1} from these injections are 0.56 and 0.91, respectively. The ^{3}He intensity gradually declines before the end of November 23. Using the LASCO CME catalog, we searched for November CMEs that preceded these ion injections. We looked for CMEs with angular widths $\geq$60° and the position angle (PA; measured from north counterclockwise) of 0°–33° or 213°–360°. CMEs with PAs like this would travel toward the

hemisphere in which Solar Orbiter is located. Six CMEs met these criteria. These CMEs, whose linear speed varied between $\sim$100 and $\sim$300 km s^{-1}, would travel to distances of 0.3–1.8 au at the liftoff time of the CME associated with the SEP event studied here. Therefore, the medium was appropriate for the confinement of ^{3}He ions from prior events. However, the CME source AR 12790 lies about 100° from the AR 12784/786 complex that produced the impulsive ^{3}He-rich events. Because the CME caused the SEP event on PSP, whose magnetic footpoint is located farther west from the AR 12786/785 complex (see Fig. 8), we assume that a broad shock from the CME extending well to the west into the reservoir accelerated the ^{3}He seed particles.

In order to determine whether ^{3}He was produced in the parent AR or in other sites on the Sun, we indicate that the examined event was accompanied by a type III radio burst and the causative electrons, commonly seen in ^{3}He-rich SEP events. Unfortunately, we lack EUV imaging observation for a detailed examination of a possible jet activity behind the limb (from the STEREO-A perspective). Cane et al. (2006, 2010) pointed out that the presence of type III radio emission in GSEP events implies that ions accelerated in a concomitant flare can escape into interplanetary space. A direct magnetic connection of Solar Orbiter with the parent AR (see Fig. 8) might allow ion escape and their measurement in the November 24 event. Previously, Cane et al. (1991) suggested that enhanced heavy-ion abundances measured in well-connected GSEP events had a component from flare-accelerated particles. In the examined event, the Fe/O is consistent with GSEP events. The obvious temporal correlation between the ^{3}He and other elements shown in detail in Fig. 5 indicates that the increased intensities are related to a single source. To argue that the ^{3}He somehow appeared with just this timing and intensity as a result of independent activities requires constructing a very unlikely scenario. Therefore, we conclude that the most likely origin of the observed ^{3}He enhancement is due to remnant material from a preceding long period of ^{3}He-rich SEP injections.

A noteworthy feature in the examined period was the storm type III bursts observed by STEREO-A. It has been suggested that storm type III bursts (Fainberg & Stone 1970) are caused by trapped solar energetic electron beams on the coronal loops (e.g., Gopalswamy et al. 2004). It seems improbable that these closed sites provide suprathermal ^{3}He for accelerations in GSEP events.

References

Bougeret, J. L., Goetz, K., Kaiser, M. L., et al. 2008, Space Sci. Rev., 136, 487
Bučík, R., Mason, G. M., Gómez-Herrero, R., et al. 2021, A&A, 656, L11
Cane, H. V., Reames, D. V., & von Rosenvinge, T. T. 1991, ApJ, 373, 675
Cane, H. V., von Rosenvinge, T. T., Cohen, C. M. S., & Mewaldt, R. A. 2003, Geophys. Res. Lett., 30, 8017
Cane, H. V., Mewaldt, R. A., Cohen, C. M. S., & von Rosenvinge, T. T. 2006, J. Geophys. Res. (Space Phys.), 111, A06S90
Cane, H. V., Richardson, I. G., & von Rosenvinge, T. T. 2010, J. Geophys. Res. (Space Phys.), 115, A08101
Cohen, C. M. S., Mewaldt, R. A., Leske, R. A., et al. 1999, Geophys. Res. Lett., 26, 2697
Desai, M., & Giacalone, J. 2016, Liv. Rev. Sol. Phys., 13, 3
Desai, M. I., Mason, G. M., Gold, R. E., et al. 2006, ApJ, 649, 470
Desai, M. I., Mason, G. M., Dayeh, M. A., et al. 2016, ApJ, 816, 68
Fainberg, J., & Stone, R. G. 1970, Sol. Phys., 15, 222
Gloeckler, G., & Geiss, J. 1998, Space Sci. Rev., 84, 275
Gopalswamy, N. 2004, in Astrophys. Space Sci. Lib., 314, 305
Hill, M. E., Mitchell, D. G., Andrews, G. B., et al. 2017, J. Geophys. Res. (Space Phys.), 122, 1513
Horbury, T. S., O'Brien, H., Carrasco Blazquez, I., et al. 2020, A&A, 642, A9
Howard, R. A., Moses, J. D., Vourlidas, A., et al. 2008, Space Sci. Rev., 136, 67
Kahler, S. W., & Brown, D. 2021, ApJ, 908, 214
Ko, Y.-K., Tylka, A. J., Ng, C. K., Wang, Y.-M., & Dietrich, W. F. 2013, ApJ, 776, 92
Kollhoff, A., Kouloumvakos, A., Lario, D., et al. 2021, A&A, 656, A20
Maksimovic, M., Bale, S. D., Chust, T., et al. 2020, A&A, 642, A12
Mann, G., Jansen, F., MacDowall, R. J., Kaiser, M. L., & Stone, R. G. 1999, A&A, 348, 614
Mason, G. M. 2007, Space Sci. Rev., 130, 231
Mason, G. M., Cohen, C. M. S., Cummings, A. C., et al. 1999a, Geophys. Res. Lett., 26, 141
Mason, G. M., Mazur, J. E., & Dwyer, J. R. 1999b, ApJ, 525, L133
Mason, G. M., Dwyer, J. R., & Mazur, J. E. 2000, ApJ, 545, L157
Mason, G. M., Nitta, N. V., Cohen, C. M. S., & Wiedenbeck, M. E. 2009, ApJ, 700, L56
Müller, D., St. Cyr, O. C., Zouganelis, I., , et al. 2020, A&A, 642, A1
Nitta, N. V., Reames, D. V., De Rosa, M. L., et al. 2006, ApJ, 650, 438
Ogilvie, K. W., Coplan, M. A., Bochsler, P., & Geiss, J. 1980, J. Geophys. Res., 85, 6021
Owen, C. J., Bruno, R., Livi, S., et al. 2020, A&A, 642, A16
Reames, D. V. 1995, Rev. Geophys., 33, 585
Reames, D. V. 2013, Space Sci. Rev., 175, 53
Reames, D. V. 2021a, Space Sci. Rev., 217, 72
Reames, D. V. 2021b, Solar Energetic Particles (Cham: Springer), 978
Robbrecht, E., Berghmans, D., & Van der Linden, R. A. M. 2009, ApJ, 691, 1222
Rochus, P., Auchère, F., Berghmans, D., et al. 2020, A&A, 642, A8
Rodríguez-Pacheco, J., Wimmer-Schweingruber, R. F., Mason, G. M., et al. 2020, A&A, 642, A7
Roelof, E. C., Gold, R. E., Simnett, G. M., et al. 1992, Geophys. Res. Lett., 19, 1243
Schatten, K. H., Wilcox, J. M., & Ness, N. F. 1969, Sol. Phys., 6, 442
Schrijver, C. J., & De Rosa, M. L. 2003, Sol. Phys., 212, 165
Tylka, A. J., Cohen, C. M. S., Dietrich, W. F., et al. 2005, ApJ, 625, 474
Von Rosenvinge, T. T., Cohen, C. M. S., Christian, E. R., et al. 2000, AIP Conf. Ser., 528, 111
Wiedenbeck, M. E., Christian, E. R., Cohen, C. M. S., et al. 2000, AIP Conf. Ser., 528, 107
Wimmer-Schweingruber, R. F., Janitzek, N. P., Pacheco, D., et al. 2021, A&A, 656, A22
Yashiro, S., Gopalswamy, N., Michalek, G., et al. 2004, J. Geophys. Res. (Space Phys.), 109, A07105